

Field-free perpendicular magnetization switching by altermagnet with collinear spin current

M. Q. Dong,¹ Zhi-Xin Guo,^{2,*} and Xin-Gao Gong^{1,†}

¹*Key Laboratory of Computational Physical Sciences (Ministry of Education),
Institute of Computational Physical Sciences,
State Key Laboratory of Surface Physics, and Department of Physics,
Fudan University, Shanghai 200433, China*

²*State Key Laboratory for Mechanical Behavior of Materials,
School of Materials Science and Engineering,
Xi'an Jiaotong University, Xi'an, Shanxi 710049, China*

(Dated: June 16, 2025)

The generation of collinear spin current (CSC), where both the propagation direction and spin-polarized direction aligned perpendicularly to the applied charge current, is crucial for efficiently manipulating systems with perpendicular magnetic anisotropy used in high-density magnetic recording. However, the efficient generation of CSC remains a challenge. In this work, based on the symmetry analysis, we propose that CSC can be effectively generated using altermagnets when the charge current is aligned along specific directions, due to spin-dependent symmetry breaking. This proposal is supported by density functional theory (DFT) and Boltzmann transport equation (BTE) calculations on a series of altermagnetic materials, including RuO₂, Mn₅Si₃, KRu₄O₈ and CuF₂, where unusually large CSC is produced by the charge current along certain orientations. Furthermore, we introduce a physical quantity, the spin-splitting angle, to quantify the efficiency of CSC generated by the charge current. We find that the spin-splitting angle ranges from 0.24 to 0.57 in these altermagnets, which is significantly larger than the spin-Hall angle typically observed in the anomalous spin-Hall effect, where the spin-Hall angle is generally less than 0.1. Our findings provide an effective method for manipulating spin currents, which is advantageous for the exploration of altermagnetic spintronic devices with field-free perpendicular magnetization switching.

INTRODUCTION

One of the most well-known applications of spintronics is electrically controllable non-volatile magnetic random-access memory (MRAM) [1, 2]. For early MRAM devices, electrical writing in multilayer structures such as spin valves and tunnel junctions is realized by

injecting spin-polarized electrons from a "pinned" ferromagnet into a "free" ferromagnetic layer through a nonmagnetic insulating layer, inducing the so-called spin transfer torque (STT) [3–7]. However, since the spin-polarized electrons pass directly through the insulating layer, this writing process does not meet the requirements for low power consumption and high speed. The spin Hall effect (SHE), which arises from spin-orbit coupling (SOC), allows an in-plane charge current to generate an out-of-plane spin current with in-plane spin polarization, thereby exerting a torque on the adjacent ferromagnetic (FM) layer [8–10]. This effect, referred to as spin-orbit torque (SOT), overcomes the limitations of STT and has garnered significant attention over the past decade [11–20]. Nevertheless, the SOT mechanisms for switching a perpendicularly magnetized system are non-deterministic [19, 21], which significantly limits their commercial applications, as materials with perpendicular magnetic anisotropy are essential for data storage media [22].

To manipulate perpendicular magnetization deterministically, an external assisting magnetic field [19, 21] or effective field [23–27] along the current direction have been proposed. However, from the perspective of commercial viability, it is essential to develop new techniques for perpendicular magnetization switching that do not rely on external magnetic or effective fields (field-free switching). Recently, the anomalous spin-Hall effect (ASHE) has been discovered, which can generate spin currents with both the propagation direction and the spin-polarized direction aligned perpendicularly to the applied charge current (denoted as *collinear spin current*, CSC), thereby enabling field-free switching [28–36]. Nevertheless, the ASHE is generally much weaker than the SHE [32, 37, 38], leading to a very small spin-Hall angle for the collinear spin current. This limitation necessitates a large current density to achieve deterministic switching, which does not align with the requirements for low power consumption. Moreover, the spin non-conserving nature of SOC, which allows for spin-current generation, simultaneously reduces the spin diffusion length, typically to the nanoscale, thereby further constraining the practical application of SOT [8]. Consequently, there is a pressing need to explore new micromechanics that can effectively generate collinear spin currents for the advancement of high-performance MRAM devices.

Recently, a novel magnetic phase termed *altermagnetism* has been both theoretically proposed and experimentally verified [39–48]. Unlike conventional collinear antiferromagnets, where opposite spin sub-lattices are connected through spatial translation (τ) or spatial inversion symmetries (\mathcal{P}), *altermagnets* link the sub-lattices through crystal-rotation (proper or improper) symmetries (\mathcal{R}) [39–42]. This unique symmetry results in spin-momentum locking (spin splitting) in momentum space, which generates a spin current when an external electric field is applied, similar to the SHE but without the involvement of SOC [48]. This characteristic introduces a new spin-splitting torque (SST) mechanism that combines the advantageous features of both STT and SOT, presenting significant potential for applications in low-power MRAM devices. However, to date, only SST based on non-collinear

spin currents (where the spin current and spin polarization are perpendicular to each other) has been discovered, which still does not enable deterministic switching of perpendicular magnetization [49, 50].

In this work, we propose that by manipulating the direction of the Néel vector in altermagnets, a collinear spin current can be effectively obtained without SOC, enabling high-efficiency deterministic switching of perpendicular magnetization. We first demonstrate the feasibility of producing such a CSC through a theoretical analysis of several altermagnets. Subsequently, using density functional theory (DFT) and Boltzmann transport equation (BTE) calculations, we reveal the unusually high efficiency of the CSC generated in altermagnets, which significantly surpasses that produced by the ASHE. This finding paves the way for the development of high-performance, low-power MRAM devices.

RESULT

Firstly, we illustrate the micromechanics of generating spin current through spin splitting in altermagnets. In general, the symmetric operations of non-relativistic spin groups can be expressed as $[\mathbf{R}_i || \mathbf{R}_j]$ [39, 51, 52], where the element on the left side (\mathbf{R}_i) of the double vertical bar is a spin space operation, and the element on the right side (\mathbf{R}_j) denotes a real-space crystallographic operation. For collinear spin arrangements in crystals, the spin group includes the symmetric operation $[E || \mathcal{T}]$, where E is the identity operation on the spin-space coordinates (\mathbf{s}) and \mathcal{T} flips the sign of the crystal momentum (\mathbf{k}). Consequently, one can derive the relation: $[E || \mathcal{T}]\epsilon(\mathbf{k}, \mathbf{s}) = \epsilon(-\mathbf{k}, \mathbf{s})$, and thus,

$$\epsilon(\mathbf{k}, \mathbf{s}) = \epsilon(-\mathbf{k}, \mathbf{s}) \quad (1)$$

for all non-relativistic collinear magnets, since $[E || \mathcal{T}]$ is a symmetric operation applicable to non-relativistic collinear spin arrangements in crystals [39]. For traditional collinear antiferromagnetic (AFM) materials, the opposite spin sub-lattices are connected through translation $[C_2 || \tau]$ or inversion $[C_2 || \mathcal{P}]$ symmetries (where C_2 transforms spin \mathbf{s} into $-\mathbf{s}$). Since $\tau\epsilon(\mathbf{k}, \mathbf{s}) = \epsilon(\mathbf{k}, \mathbf{s})$ and $\mathcal{P}\epsilon(\mathbf{k}, \mathbf{s}) = \epsilon(-\mathbf{k}, \mathbf{s})$, it follows that $[C_2 || \tau]\epsilon(\mathbf{k}, \mathbf{s}) = \epsilon(\mathbf{k}, -\mathbf{s})$ and $[C_2 || \mathcal{P}]\epsilon(\mathbf{k}, \mathbf{s}) = \epsilon(-\mathbf{k}, -\mathbf{s})$. Combining these with Eq. (1), we can derive:

$$\epsilon(\mathbf{k}, \mathbf{s}) = \epsilon(\mathbf{k}, -\mathbf{s}), \quad (2)$$

which indicates that the energy bands of different spins are degenerate at every point in the Brillouin zone. As a result, when an external electric field is applied, the electrons of different spins respond identically to the electric field, which naturally does not produce spin-polarized currents.

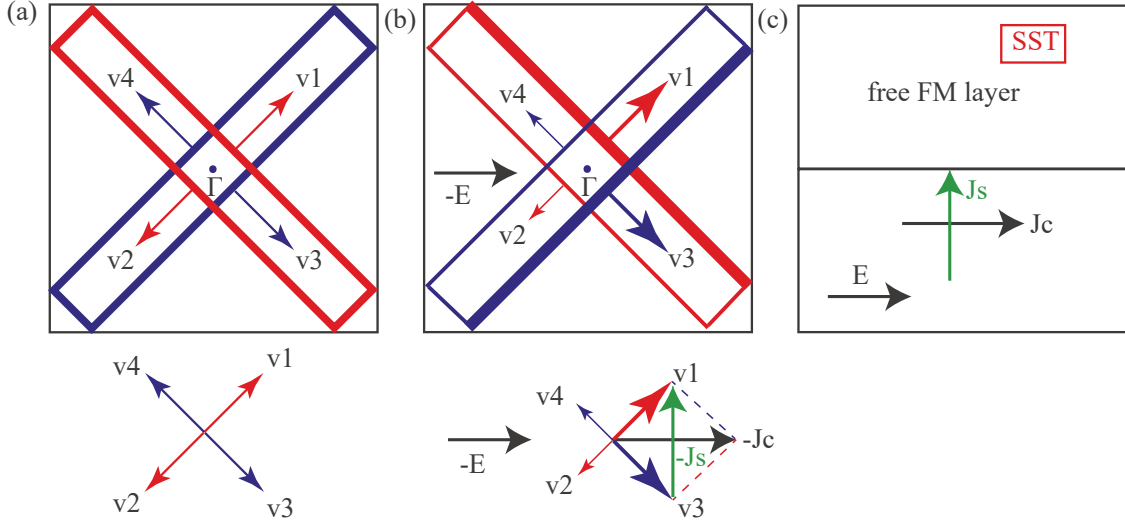


FIG. 1. (a) Simplified Fermi surface of $[C_2||C_{4z}]$ altermagnet in the absence of electric field. The red and blue lines represent the Fermi surfaces of spin-up and spin-down electrons, respectively. The red and blue arrows illustrate the Fermi velocity of spin-up electrons and spin-down electrons, correspondingly. (b) Redistribution of electrons at the Fermi surface induced by the application of an electric field, indicated by variations in line thickness. The green arrows depict the associated spin currents. (c) Schematic diagram illustrating the generation of collinear spin current (CSC, J_s) under external electric field and CSC applied spin-splitting torque (SST) to the adjacent ferromagnetic layer.

In contrast, for altermagnets, the situation is different, as their sub-lattices are linked by crystal-rotation (proper or improper) symmetries, i.e., $[C_2||C_n]$ or $[C_2||\mathbf{m}]$ (C_n represents n -fold ($n > 1$) rotation operation, and \mathbf{m} represents spatial mirror operation). Note that the spatial translation operation τ is disregarded here, as it has no effect on the band structure. Considering that $C_n\epsilon(\mathbf{k}, \mathbf{s}) = \epsilon(C_n\mathbf{k}, \mathbf{s})$ and $\mathbf{m}\epsilon(\mathbf{k}, \mathbf{s}) = \epsilon(\mathbf{m}\mathbf{k}, \mathbf{s})$, one can obtain $[C_2||C_n]\epsilon(\mathbf{k}, \mathbf{s}) = \epsilon(C_n\mathbf{k}, -\mathbf{s})$ and $[C_2||\mathbf{m}]\epsilon(\mathbf{k}, \mathbf{s}) = \epsilon(\mathbf{m}\mathbf{k}, -\mathbf{s})$, we can derive:

$$\epsilon(\mathbf{k}, \mathbf{s}) = \epsilon(\mathbf{k}', -\mathbf{s}), \quad (3)$$

for altermagnets, where \mathbf{k}' is obtained from \mathbf{k} by C_n or \mathbf{m} operations. This means that a state with spin \mathbf{s} at general position \mathbf{k} in the Brillouin zone must correspond to a state with spin $-\mathbf{s}$ at another position \mathbf{k}' in the Brillouin zone. Consequently, electrons with different spins can form distinct currents when an external electric field is applied in a specific direction, resulting in a spin-polarized current. It is important to note that the improper rotation in this context should not include the spatial inversion operation \mathcal{P} ; otherwise, one cannot obtain the spin current induced by spin splitting, as is the case in conventional AFM materials [39].

In the absence of an external electric field, i.e., under equilibrium conditions, the electrons

are symmetrically distributed in momentum space, and their velocities ($\mathbf{v}_{n\mathbf{k}} = \partial\epsilon_n(\mathbf{k})/\partial\mathbf{k}$) along all directions cancel each other out. As a result, the integral of the velocity of all electrons is zero. Consequently, the integral of the spin times the velocity of all electrons ($\int \mathbf{s}\mathbf{v} d^3\mathbf{k}$) also equals zero, indicating that there is no macroscopic charge current or spin current, as illustrated in Fig. 1(a). On the other hand, when an external electric field is present, the distribution function of electrons near the Fermi level experiences a slight shift in the opposite direction of the electric field [see Fig. 1(b)]. At this point, the electron velocities along all directions can no longer cancel out. As a result, in addition to the longitudinal charge current, a net transverse spin current is also generated by the external electric field, as indicated in Fig. 1(b). In particular, in altermagnetic materials, when the Néel vector is perpendicular to the external electric field, the electric field (e.g., in the x -direction) will induce a transverse CSC (e.g., in the y/z direction). This CSC can produce a significant SST, which is injected into the adjacent ferromagnetic (FM) layer to achieve high-efficiency deterministic switching of perpendicular magnetization, as shown in Fig. 1(c).

We further discuss the electronic transport properties of altermagnets, which directly correlate to the characteristic of band splittings discussed above. Here, a spin conductance $\sigma_{\alpha\beta}^{\gamma\uparrow}(\sigma_{\alpha\beta}^{\gamma\downarrow})$ is defined, where α represents the propagation direction of spin current, β means the direction of external electric field, and γ is the direction of spin polarization, respectively. Note that “ \uparrow ” and “ \downarrow ” represent the spin-up and spin-down electrons, respectively. In altermagnets exhibiting symmetric operations such as $[E||C_{2z}]$ or $[E||C_{2z}\tau]$, one can derive the relation: $[E||C_{2z}]\epsilon(k_x, k_y, k_z, \mathbf{s}) = \epsilon(-k_x, -k_y, k_z, \mathbf{s})$ and thus $\epsilon(k_x, k_y, k_z, \mathbf{s}) = \epsilon(k_x, k_y, -k_z, \mathbf{s})$ by combining with Eq. (1). In other words, the band structures of both spin-up and spin-down electrons exhibit \mathbf{m}_z mirror symmetry with respect to the momentum space of the $k_z = 0$ plane. Therefore, two of the three transverse components of electronic conductivity, namely, $\sigma_{zx}^{\gamma\uparrow}(\sigma_{zx}^{\gamma\downarrow})$ and $\sigma_{zy}^{\gamma\uparrow}(\sigma_{zy}^{\gamma\downarrow})$, must be zero, and only $\sigma_{yx}^{\gamma\uparrow}(\sigma_{yx}^{\gamma\downarrow})$ can be non-zero, where $\gamma = x, y, z$, representing the direction of spin polarization (see section SI and SII of Supplementary Material for details [53]).

For convenience in discussing the physics of CSC, we denote the direction of the external electric field (or charge current) as the x -direction (E_x). Then, a spin current transporting along α -direction ($\alpha = x, y, z$) with spin polarization along γ -direction ($\alpha = x, y, z$), i.e., $J_{\alpha x}^{\gamma}$, can be generally defined as [67]

$$J_{\alpha x}^{\gamma} = (\sigma_{\alpha x}^{\gamma\uparrow} - \sigma_{\alpha x}^{\gamma\downarrow})E_x. \quad (4)$$

Note that when the external electric field is oriented along other directions (e.g., E_y and E_z), one can also obtain non-zero CSC using a similar analytical approach. As shown in Eq. (4), a non-zero $(\sigma_{\alpha x}^{\gamma\uparrow} - \sigma_{\alpha x}^{\gamma\downarrow})$ implies that when an electric field is applied in the x -direction, a non-zero spin current in the y -direction can be generated, i.e., $J_{yx}^{\gamma} \neq 0$. It is noted that

the spin polarization of most conduction electrons in a magnetic material is parallel to the magnetization direction, i.e., the Néel vector in altermagnets [49, 50]. Hence, a sizable non-zero CSC of $J_{yx}^y (J_{zx}^z)$ can be achieved when the Néel vector is oriented along the y -direction (z -direction) [49], provided by $\sigma_{yx}^{y\uparrow} - \sigma_{yx}^{y\downarrow} \neq 0$ ($\sigma_{zx}^{z\uparrow} - \sigma_{zx}^{z\downarrow} \neq 0$).

Accordingly, for altermagnets exhibiting symmetric operations such as $[C_2||\mathbf{m}_z]$ or $[C_2||\mathbf{m}_z\tau]$, one can derive the relation $[C_2||\mathbf{m}_z]\epsilon(k_x, k_y, k_z, \mathbf{s}) = \epsilon(k_x, k_y, -k_z, -\mathbf{s})$. This means that the band structure of spin-up electrons and spin-down electrons are connected via \mathbf{m}_z mirror symmetry with respect to momentum space of $k_z = 0$ plane. Specifically, this leads to the relations $\sigma_{yx}^{y\uparrow} = \sigma_{yx}^{y\downarrow}$ and $\sigma_{zx}^{z\uparrow} = -\sigma_{zx}^{z\downarrow}$ (section SII of Supplementary Material [53]). As a result, $J_{yx}^y = 0$ but $J_{zx}^z \neq 0$, indicating that a non-zero CSC with both spin propagation and spin polarization directions along the z -direction can also be obtained when the Néel vector is oriented along the z -direction.

To verify the theoretical derivations presented above, we further perform DFT calculations (see Supplementary Material [53] for details) on several metallic altermagnets, including RuO_2 , KRu_4O_8 and Mn_5Si_3 , which exhibit symmetric operation $[E||C_{2z}]$ or $[E||C_{2z}\tau]$. Additionally, we consider an insulating altermagnet, CuF_2 that has the symmetric operation $[C_2||\mathbf{m}_z\tau]$, for comparison.

The atomic structures of the four altermagnets are presented in Fig. 2. RuO_2 is a rutile oxide that belongs to the tetragonal $P4_2/mnm$ space group, consisting of two collinear opposite spin sub-lattices linked by a 4-fold crystal-rotation operation $[C_2||C_{4z}\tau]$ [Fig. 2(a)]. KRu_4O_8 features a hollandite structure that belongs to the centered tetragonal $I4/m$ space group and exhibits a collinear AFM ground state, with opposite sub-lattices connected by a 4-fold crystal-rotation operation $[C_2||C_{4z}]$ [Fig. 2(b)]. Mn_5Si_3 has a space group of $P6_3/mcm$, characterized by a hexagonal unit cell containing two formula units [Fig. 2(c)], i.e., four Mn atoms (Mn_1) located at the Wyckoff position 4d, and six Mn atoms (Mn_2) at the Wyckoff position 6g (two Mn_2 atoms are nonmagnetic) [68–70]. As for the CuF_2 , it belongs to the monoclinic $P2_1/b$ space group consists of two collinear opposite spin sub-lattices linked by either a 2-fold crystal-rotation operation $[C_2||C_{2z}\tau]$ or mirror operation $[C_2||\mathbf{m}_z\tau]$ [Fig. 2(d)] [71, 72]. As shown below, although these altermagnetic materials have distinct atomic structures and belong different space groups, a common feature is that their band structures present significant band splitting along certain path in the Brillouin zone.

Figure 3 presents the DFT-calculated spin-polarized band structures of the four altermagnets discussed above. It is observed that the band structures of RuO_2 and KRu_4O_8 exhibit symmetric spin splitting along the paths M1- Γ -M2 and A1-Z-A2, while displaying spin degeneracy along the path Z- Γ [Figs. 3(a) and 3(b)]. This result aligns well with the symmetry analysis based on the spin group operation $[C_2||C_{4z}\tau]$ or $[C_2||C_{4z}]$ for RuO_2 and KRu_4O_8 . On the other hand, Mn_5Si_3 exhibits a symmetric operation $[C_2||\mathbf{m}_y]$. According to the symmetry analysis, its band structure should show spin splitting along the

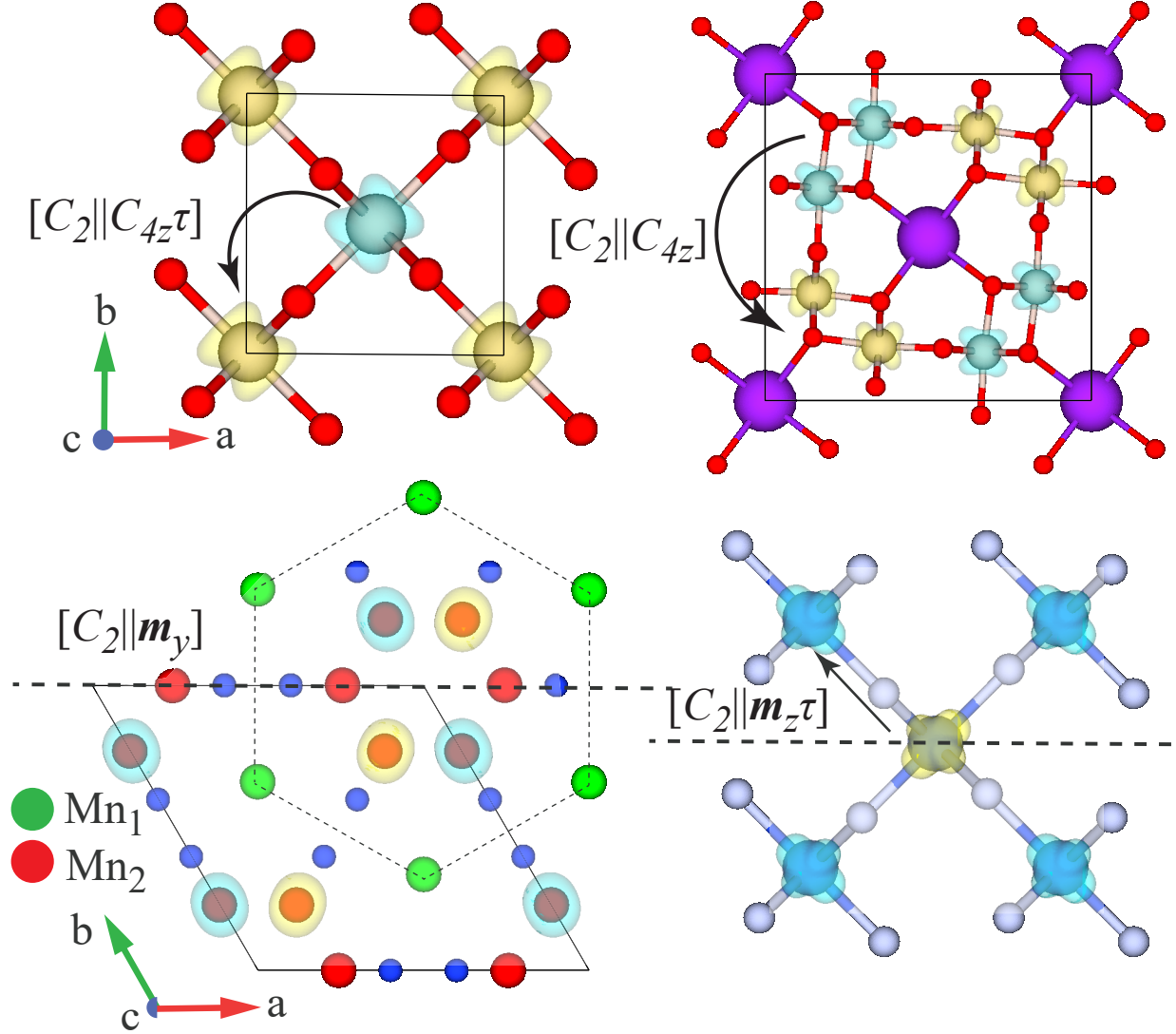


FIG. 2. Atomic structures, spin density distributions, and permitted alternating symmetric operations for (a) RuO_2 , (b) KRu_4O_8 , (c) Mn_5Si_3 and (d) CuF_2 .

paths K4- Γ -K1 and K2-K3, while demonstrating spin degeneracy along the paths K1-K2 and K3-K4. As illustrated in Fig. 3(c), the DFT-calculated band structure confirms these characteristics. As for CuF_2 , which possesses a mirror operation of $[C_2||\mathbf{m}_z\tau]$, one can derive the relations: $[C_2||\mathbf{m}_z\tau]\epsilon(k_x, k_y, k_z = 0, \mathbf{s}) = \epsilon(k_x, k_y, k_z = 0, -\mathbf{s})$ and $[C_2||\mathbf{m}_z\tau]\epsilon(k_x, k_y, k_z = \pi, \mathbf{s}) = \epsilon(k_x, k_y, k_z = -\pi, -\mathbf{s}) = \epsilon(k_x, k_y, k_z = \pi, -\mathbf{s})$. This indicates that its band structure exhibits spin degeneracy in the Brillouin zone planes at $k_z = 0$ and $k_z = \pi$. Therefore, we analyze the Brillouin zone plane at $k_z = \pi/2$ to illustrate its spin band-splitting characteristics, where band splitting is expected to occur along the D1- Γ -D2 and C1-C2 paths, respectively, in accordance with the mirror operation $[C_2||\mathbf{m}_z\tau]$ and the crystal-rotation operation $[C_2||C_{2z}\tau]$. As shown in Fig. 3(d), this feature is also consistent with the DFT

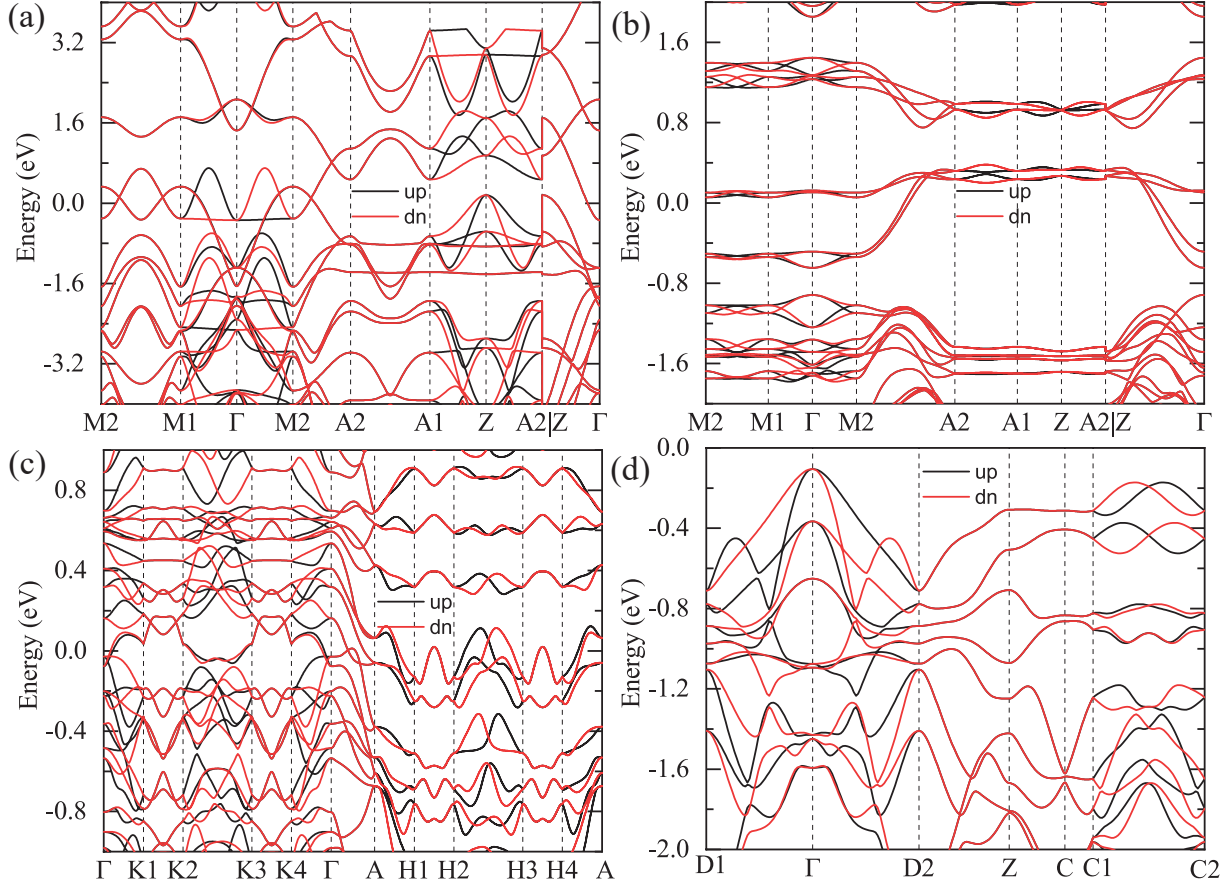


FIG. 3. Band structures along high-symmetry paths for (a) RuO_2 , (b) KRu_4O_8 , (c) Mn_5Si_3 and (d) CuF_2 . The shape of the Brillouin zone and the coordinates of the high-symmetry points are provided in the section SIII of Supplemental Materials [53].

calculations.

To more clearly illustrate the symmetry-correlated electronic structures of the altermagnets, we also calculate the isoenergetic surfaces of the four altermagnetic materials discussed above. As shown in Fig. 4, the isoenergetic surfaces of RuO_2 (at $E = E_F = 0$) and CuF_2 (at $E = -0.27$ eV) exhibit symmetry along certain directions in the Brillouin zone, which aligns well with the symmetry analysis discussed earlier. Note that in CuF_2 the non-zero energy level of isoenergetic surface is adopted, because it is an insulator [Fig. 3(d)]. It is noteworthy that good agreement between the isoenergetic surface profiles and the symmetry analysis is also obtained in KRu_4O_8 and Mn_5Si_3 at E_F (section SIV of Supplemental Materials [53]). Since the spin-splitting energy is generally at eV level, which is significantly greater than that induced by the SOC effect (typically at the meV level), the spin splitting in altermagnets is expected to generate a much more substantial CSC than that produced by ASHE. This makes altermagnets highly promising for applications in MRAM devices.

We now turn to the discussion of the spin transport properties of the above four alter-

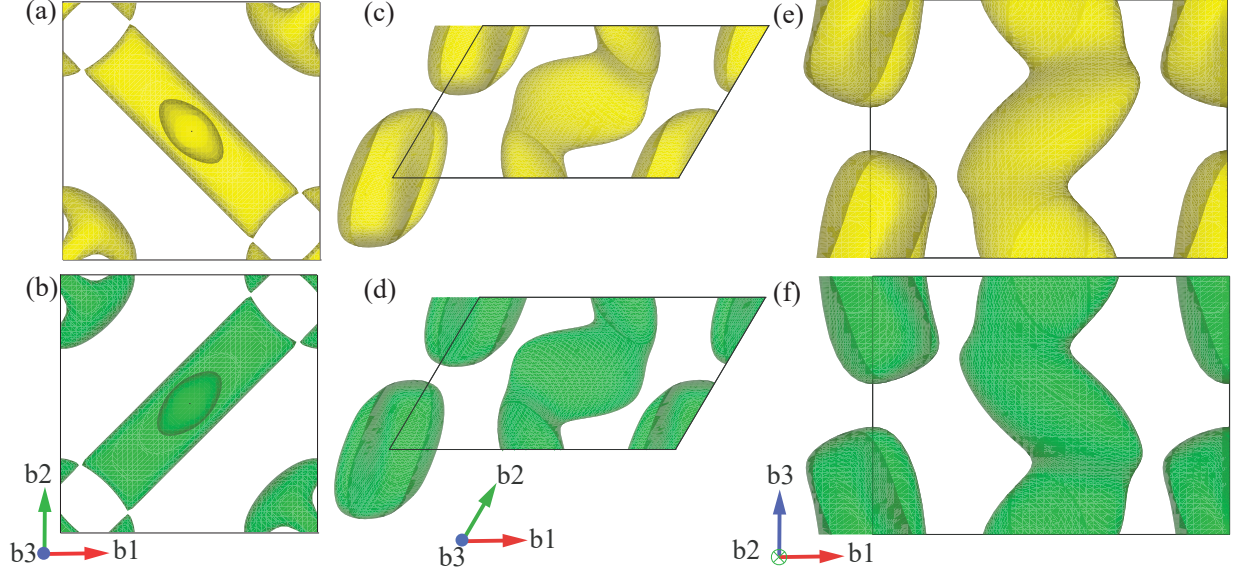


FIG. 4. Isoenergetic surface of RuO_2 ($E = E_F$) and CuF_2 ($E = -0.27$ eV). (a) Top view of spin-up electrons of RuO_2 . (b) Top view of spin-down electrons of RuO_2 . (c) Top view of spin-up electrons of CuF_2 . (d) Top view of spin-down electrons of CuF_2 . (e) Side view of spin-up electrons of CuF_2 and (f) side view of spin-down electrons of CuF_2 . Isoenergetic surface of KRu_4O_8 and Mn_5Si_3 are presented in the Supplemental Materials [53].

magnets. Figures 5(a) and 5(b) display the calculated longitudinal electric conductivity and transverse conductivity of RuO_2 , with the charge current oriented along the [100] direction (x -direction) (see section SI of Supplementary Material for calculation details [53]). It is observed that spin-up electrons and spin-down electrons exhibit the same longitudinal conductivity but have opposite transverse conductivity. Consequently, a net longitudinal charge current $J_{xx} = (\sigma_{xx}^{\uparrow} + \sigma_{xx}^{\downarrow})E_x$ is generated in the x -direction, and a net transverse spin current $J_{yx}^{\gamma} = (\sigma_{yx}^{\uparrow} - \sigma_{yx}^{\downarrow})E_x$ is produced in the [010] direction (y -direction). Since the spin polarization direction γ is aligned along the Néel vector, a net CSC (J_{yx}^y) would be obtained in RuO_2 when the Néel vector is along [010] direction.

In a manner analogous to the definition of the spin Hall angle [8], we further introduce a physical quantity, *spin-splitting angle* (α), to quantify the conversion efficiency from charge current to CSC resulting from spin splitting [48]. It is important to note that the spin-splitting angle is a tensor. For instance, for a CSC in the y -direction (the Néel vector is along y -direction) induced by electric field in x -direction, it can be expressed as:

$$\alpha_{yx} = \left| \frac{J_{yx}^{\gamma}}{J_{xx}} \right| = \left| \frac{\sigma_{yx}^{\uparrow} - \sigma_{yx}^{\downarrow}}{\sigma_{xx}^{\uparrow} + \sigma_{xx}^{\downarrow}} \right|. \quad (5)$$

From Figs. 5(a) and 5(b), one can observe a large spin splitting angle α_{yx} of approximately 0.57 at the E_F for RuO_2 . This indicates that the charge-to-spin transfer efficiency for the

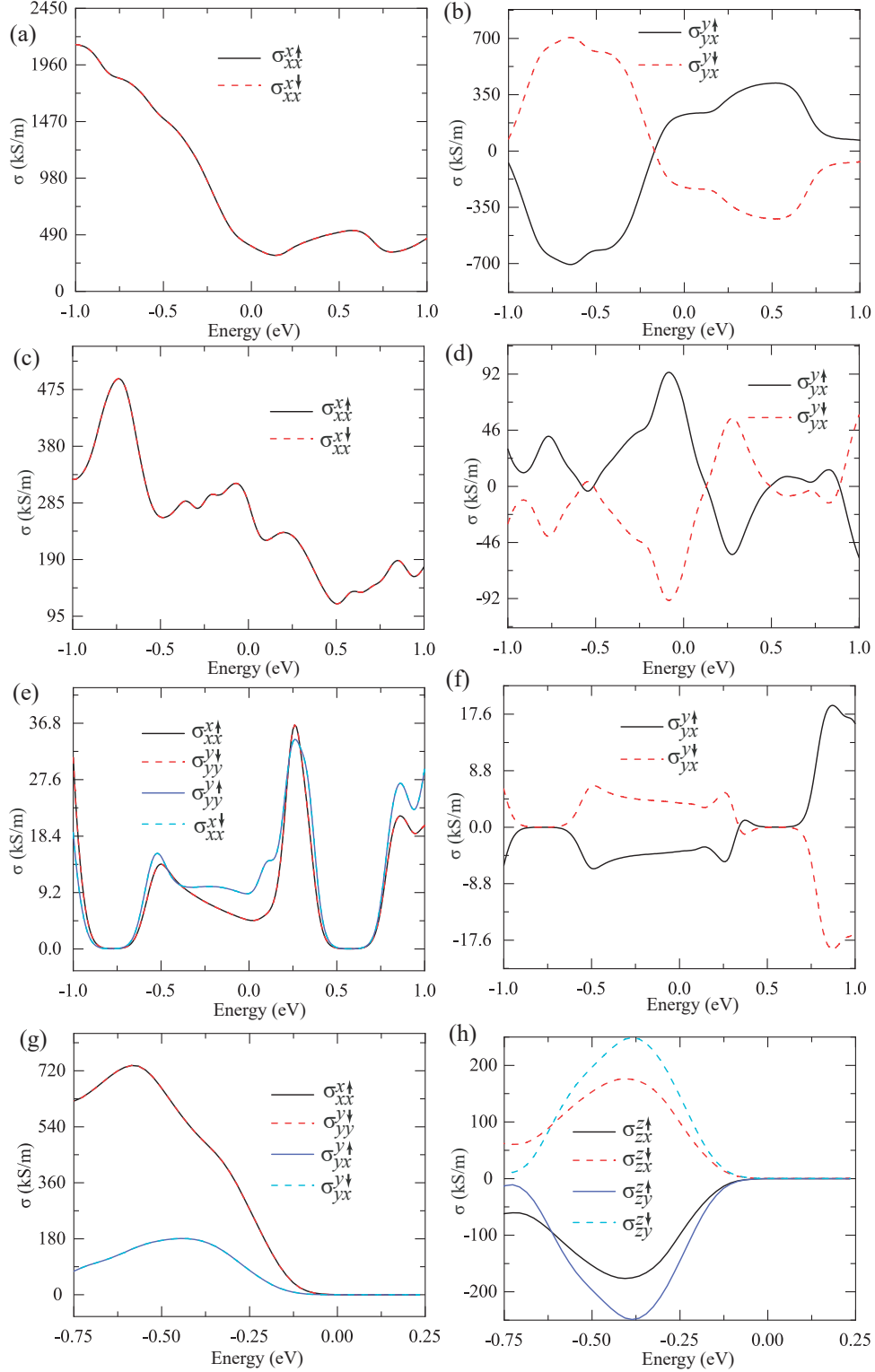


FIG. 5. Calculated conductivity for RuO_2 (a-b), Mn_5Si_3 (c-d), KRu_4O_8 (e-f), CuF_2 (g-h). For RuO_2 , Mn_5Si_3 and KRu_4O_8 , the calculated $\sigma_{zx}^{\uparrow/\downarrow}$ and $\sigma_{zy}^{\uparrow/\downarrow}$ are both zero for spin-up electrons and spin-down electrons.

CSC is several dozen times greater than that produced via ASHE (0.013 [32]), highlighting the significant potential of altermagnets in SST-MRAM devices. It is noteworthy that the calculated transverse spin conductivity in the z -direction is zero for both spin-up electrons ($\sigma_{zx}^{z\uparrow} = 0$) and spin-down electrons ($\sigma_{zx}^{z\downarrow} = 0$), resulting in $\alpha_{zx} = 0$. This result is also consistent with the symmetry analysis, i.e., the band structures of both spin-up and spin-down electrons exhibit \mathbf{m}_z mirror symmetry. Additionally, according to the symmetry analysis, Mn_5Si_3 and KRu_4O_8 would exhibit a non-zero CSC and thus α_{yx} in the y -direction ($[0\bar{1}\bar{1}0]$ for Mn_5Si_3 and $[010]$ for KRu_4O_8) when the external electric field is applied along the $[2\bar{1}\bar{1}0]$ and $[100]$ directions (denoted as x -direction) for Mn_5Si_3 and KRu_4O_8 , respectively. Figs. 5(c)-5(f) further show the calculated longitudinal and transverse spin conductivities, demonstrating that Mn_5Si_3 ($\alpha_{yx} = 0.24$) and KRu_4O_8 ($\alpha_{yx} = 0.55$) also possess sizable spin splitting-angles.

Finally, we present all the possible non-zero CSCs generated in the four altermagnets with the external electric field varying among x ($[100]$), y ($[010]$), and z ($[001]$) directions, as shown in Table I. For RuO_2 , Mn_5Si_3 and KRu_4O_8 , the CSCs in both the x and y directions can be effectively generated by appropriately choosing the direction of the charge current. In contrast, for CuF_2 , CSCs can be obtained in any of the x , y , or z direction. Combining with the unusually large spin splitting angles of these CSCs shown in Table I, these results present a promising way of realizing efficient deterministic switching using altermagnets. It is worth noting that, in addition to the CSCs propagating in the transverse direction of the charge current, a spin-polarized current in the longitudinal direction of the charge current can also be generated in KRu_4O_8 , highlighting the rich spin-transport properties of altermagnets.

TABLE I. Non-zero CSC (J_s) and spin-splitting angle (α) in RuO_2 , Mn_5Si_3 , KRu_4O_8 , and CuF_2 . M and I denote metal and insulator, respectively. For RuO_2 , Mn_5Si_3 , KRu_4O_8 , which are metals, we calculate α at the Fermi level ($E=0$).

Materials	J_s	α
RuO_2 (M)	$\begin{pmatrix} 0 & J_{xy}^x & 0 \\ J_{yx}^y & 0 & 0 \\ 0 & 0 & 0 \end{pmatrix}$	$\begin{pmatrix} 0 & 57\% & 0 \\ 57\% & 0 & 0 \\ 0 & 0 & 0 \end{pmatrix}$
Mn_5Si_3 (M)	$\begin{pmatrix} 0 & J_{xy}^x & 0 \\ J_{yx}^y & 0 & 0 \\ 0 & 0 & 0 \end{pmatrix}$	$\begin{pmatrix} 0 & 24\% & 0 \\ 24\% & 0 & 0 \\ 0 & 0 & 0 \end{pmatrix}$
KRu_4O_8 (M)	$\begin{pmatrix} J_{xx}^x & J_{xy}^x & 0 \\ J_{yx}^y & J_{yy}^y & 0 \\ 0 & 0 & 0 \end{pmatrix}$	$\begin{pmatrix} 32\% & 55\% & 0 \\ 55\% & 32\% & 0 \\ 0 & 0 & 0 \end{pmatrix}$
CuF_2 (I)	$\begin{pmatrix} 0 & 0 & J_{xz}^x \\ 0 & 0 & J_{yz}^y \\ J_{zx}^z & J_{zy}^z & 0 \end{pmatrix}$	insulator

Before concluding, we would like to remark on the effect of SOC on the CSC. In the Supplemental materials, we present the calculated conductivity of RuO₂, both with and without the SOC effect. It is found that although the conductivity is slightly reduced in the presence of SOC, the positive and negative relationship between spin-up and spin-down electrons remains largely unchanged. As a result, the spin splitting angle α_{yx} remains substantial at 0.39, demonstrating the robustness of CSC in altermagnets.

CONCLUSION

In summary, based on the symmetry analysis, we find that the spin-dependent symmetry breaking can induce non-zero CSCs when the electric field is applied along specific directions in altermagnets, such as RuO₂, Mn₅Si₃, KRu₄O₈, and CuF₂. In use of DFT and BTE calculations, we further reveal that the CSCs in either transverse or longitudinal directions can be significantly large. We find that the efficiency of charge to collinear spin current (spin spin-splitting angle) ranges from 0.24 to 0.57 in these altermagnets, significantly larger than that achieved by the anomalous spin-Hall effect. Our findings provide a technique for effectively manipulating spin currents, which is advantageous for the exploration of altermagnetic spintronic devices with field-free perpendicular magnetization switching.

ACKNOWLEDGMENTS

This work was supported by the Ministry of Science and Technology of the People's Republic of China (2024YFA1408501), Natural Science Foundation of China (Grants No. 12474237), Science Fund for Distinguished Young Scholars of Shaanxi Province (Grant No. 2024JC-JCQN-09).

* zxguo08@xjtu.edu.cn

† xggong@fudan.edu.cn

- [1] S. Wolf, D. Awschalom, R. Buhrman, J. Daughton, v. S. von Molnár, M. Roukes, A. Y. Chtchelkanova, and D. Treger, Spintronics: a spin-based electronics vision for the future, *science* **294**, 1488 (2001).
- [2] S. Bhatti, R. Sbiaa, A. Hirohata, H. Ohno, S. Fukami, and S. Piramanayagam, Spintronics based random access memory: a review, *Materials Today* **20**, 530 (2017).
- [3] J. C. Slonczewski, Current-driven excitation of magnetic multilayers, *Journal of Magnetism and Magnetic Materials* **159**, L1 (1996).

- [4] L. Berger, Emission of spin waves by a magnetic multilayer traversed by a current, *Phys. Rev. B* **54**, 9353 (1996).
- [5] D. C. Ralph and M. D. Stiles, Spin transfer torques, *Journal of Magnetism and Magnetic Materials* **320**, 1190 (2008).
- [6] A. Brataas, A. D. Kent, and H. Ohno, Current-induced torques in magnetic materials, *Nature materials* **11**, 372 (2012).
- [7] A. Khvalkovskiy, D. Apalkov, S. Watts, R. Chepulskii, R. Beach, A. Ong, X. Tang, A. Driskill-Smith, W. Butler, P. Visscher, *et al.*, Basic principles of stt-mram cell operation in memory arrays, *Journal of Physics D: Applied Physics* **46**, 074001 (2013).
- [8] A. Manchon, J. Železný, I. M. Miron, T. Jungwirth, J. Sinova, A. Thiaville, K. Garello, and P. Gambardella, Current-induced spin-orbit torques in ferromagnetic and antiferromagnetic systems, *Rev. Mod. Phys.* **91**, 035004 (2019).
- [9] J. Železný, H. Gao, A. Manchon, F. Freimuth, Y. Mokrousov, J. Zemen, J. Mašek, J. Sinova, and T. Jungwirth, Spin-orbit torques in locally and globally noncentrosymmetric crystals: Antiferromagnets and ferromagnets, *Phys. Rev. B* **95**, 014403 (2017).
- [10] A. Chernyshov, M. Overby, X. Liu, J. K. Furdyna, Y. Lyanda-Geller, and L. P. Rokhinson, Evidence for reversible control of magnetization in a ferromagnetic material by means of spin-orbit magnetic field, *Nature Physics* **5**, 656 (2009).
- [11] M. I. Dyakonov and V. Perel, Current-induced spin orientation of electrons in semiconductors, *Physics Letters A* **35**, 459 (1971).
- [12] J. E. Hirsch, Spin hall effect, *Phys. Rev. Lett.* **83**, 1834 (1999).
- [13] S. Zhang, Spin hall effect in the presence of spin diffusion, *Phys. Rev. Lett.* **85**, 393 (2000).
- [14] J. Sinova, D. Culcer, Q. Niu, N. A. Sinitsyn, T. Jungwirth, and A. H. MacDonald, Universal intrinsic spin hall effect, *Phys. Rev. Lett.* **92**, 126603 (2004).
- [15] S. Murakami, N. Nagaosa, and S.-C. Zhang, Dissipationless quantum spin current at room temperature, *Science* **301**, 1348 (2003).
- [16] T. Kimura, Y. Otani, T. Sato, S. Takahashi, and S. Maekawa, Room-temperature reversible spin hall effect, *Phys. Rev. Lett.* **98**, 156601 (2007).
- [17] I. Mihai Miron, G. Gaudin, S. Auffret, B. Rodmacq, A. Schuhl, S. Pizzini, J. Vogel, and P. Gambardella, Current-driven spin torque induced by the rashba effect in a ferromagnetic metal layer, *Nature materials* **9**, 230 (2010).
- [18] U. H. Pi, K. Won Kim, J. Y. Bae, S. C. Lee, Y. J. Cho, K. S. Kim, and S. Seo, Tilting of the spin orientation induced by rashba effect in ferromagnetic metal layer, *Applied Physics Letters* **97** (2010).
- [19] I. M. Miron, K. Garello, G. Gaudin, P.-J. Zermatten, M. V. Costache, S. Auffret, S. Bandiera, B. Rodmacq, A. Schuhl, and P. Gambardella, Perpendicular switching of a single ferromagnetic layer induced by in-plane current injection, *Nature* **476**, 189 (2011).

- [20] T. Suzuki, S. Fukami, N. Ishiwata, M. Yamanouchi, S. Ikeda, N. Kasai, and H. Ohno, Current-induced effective field in perpendicularly magnetized ta/cofeb/mgo wire, *Applied Physics Letters* **98** (2011).
- [21] L. Liu, O. J. Lee, T. J. Gudmundsen, D. C. Ralph, and R. A. Buhrman, Current-induced switching of perpendicularly magnetized magnetic layers using spin torque from the spin hall effect, *Phys. Rev. Lett.* **109**, 096602 (2012).
- [22] A. Moser, K. Takano, D. T. Margulies, M. Albrecht, Y. Sonobe, Y. Ikeda, S. Sun, and E. E. Fullerton, Magnetic recording: advancing into the future, *Journal of Physics D: Applied Physics* **35**, R157 (2002).
- [23] G. Yu, P. Upadhyaya, Y. Fan, J. G. Alzate, W. Jiang, K. L. Wong, S. Takei, S. A. Bender, L.-T. Chang, Y. Jiang, *et al.*, Switching of perpendicular magnetization by spin-orbit torques in the absence of external magnetic fields, *Nature nanotechnology* **9**, 548 (2014).
- [24] S. Fukami, C. Zhang, S. DuttaGupta, A. Kurenkov, and H. Ohno, Magnetization switching by spin-orbit torque in an antiferromagnet-ferromagnet bilayer system, *Nature materials* **15**, 535 (2016).
- [25] A. van den Brink, G. Vermaijns, A. Solignac, J. Koo, J. T. Kohlhepp, H. J. Swagten, and B. Koopmans, Field-free magnetization reversal by spin-hall effect and exchange bias, *Nature communications* **7**, 10854 (2016).
- [26] Y.-C. Lau, D. Betto, K. Rode, J. Coey, and P. Stamenov, Spin-orbit torque switching without an external field using interlayer exchange coupling, *Nature nanotechnology* **11**, 758 (2016).
- [27] K. Cai, M. Yang, H. Ju, S. Wang, Y. Ji, B. Li, K. W. Edmonds, Y. Sheng, B. Zhang, N. Zhang, *et al.*, Electric field control of deterministic current-induced magnetization switching in a hybrid ferromagnetic/ferroelectric structure, *Nature materials* **16**, 712 (2017).
- [28] S.-h. C. Baek, V. P. Amin, Y.-W. Oh, G. Go, S.-J. Lee, G.-H. Lee, K.-J. Kim, M. D. Stiles, B.-G. Park, and K.-J. Lee, Spin currents and spin-orbit torques in ferromagnetic trilayers, *Nature materials* **17**, 509 (2018).
- [29] Y. Liu and Q. Shao, Two-dimensional materials for energy-efficient spin-orbit torque devices, *ACS nano* **14**, 9389 (2020).
- [30] G. M. Stiehl, R. Li, V. Gupta, I. E. Baggari, S. Jiang, H. Xie, L. F. Kourkoutis, K. F. Mak, J. Shan, R. A. Buhrman, and D. C. Ralph, Layer-dependent spin-orbit torques generated by the centrosymmetric transition metal dichalcogenide β -mote₂, *Phys. Rev. B* **100**, 184402 (2019).
- [31] P. Song, C.-H. Hsu, G. Vignale, M. Zhao, J. Liu, Y. Deng, W. Fu, Y. Liu, Y. Zhang, H. Lin, *et al.*, Coexistence of large conventional and planar spin hall effect with long spin diffusion length in a low-symmetry semimetal at room temperature, *Nature materials* **19**, 292 (2020).
- [32] D. MacNeill, G. Stiehl, M. Guimaraes, R. Buhrman, J. Park, and D. Ralph, Control of spin-orbit torques through crystal symmetry in wte₂/ferromagnet bilayers, *Nature Physics* **13**, 300

- (2017).
- [33] D. MacNeill, G. M. Stiehl, M. H. D. Guimarães, N. D. Reynolds, R. A. Buhrman, and D. C. Ralph, Thickness dependence of spin-orbit torques generated by wte_2 , *Phys. Rev. B* **96**, 054450 (2017).
- [34] S. Shi, S. Liang, Z. Zhu, K. Cai, S. D. Pollard, Y. Wang, J. Wang, Q. Wang, P. He, J. Yu, *et al.*, All-electric magnetization switching and dzyaloshinskii–moriya interaction in wte_2 /ferromagnet heterostructures, *Nature nanotechnology* **14**, 945 (2019).
- [35] I.-H. Kao, R. Muzzio, H. Zhang, M. Zhu, J. Gobbo, S. Yuan, D. Weber, R. Rao, J. Li, J. H. Edgar, *et al.*, Deterministic switching of a perpendicularly polarized magnet using unconventional spin–orbit torques in wte_2 , *Nature materials* **21**, 1029 (2022).
- [36] P. Li, J.-Z. Zhang, Z.-X. Guo, T. Min, and X. Wang, Intrinsic anomalous spin hall effect, *Science China Physics, Mechanics & Astronomy* **66**, 227511 (2023).
- [37] L. Liu, T. Moriyama, D. C. Ralph, and R. A. Buhrman, Spin-torque ferromagnetic resonance induced by the spin hall effect, *Phys. Rev. Lett.* **106**, 036601 (2011).
- [38] L. Liu, C.-F. Pai, Y. Li, H. Tseng, D. Ralph, and R. Buhrman, Spin-torque switching with the giant spin hall effect of tantalum, *Science* **336**, 555 (2012).
- [39] L. Šmejkal, J. Sinova, and T. Jungwirth, Beyond conventional ferromagnetism and antiferromagnetism: A phase with nonrelativistic spin and crystal rotation symmetry, *Phys. Rev. X* **12**, 031042 (2022).
- [40] L. Šmejkal, J. Sinova, and T. Jungwirth, Emerging research landscape of altermagnetism, *Phys. Rev. X* **12**, 040501 (2022).
- [41] P. Liu, J. Li, J. Han, X. Wan, and Q. Liu, Spin-group symmetry in magnetic materials with negligible spin-orbit coupling, *Phys. Rev. X* **12**, 021016 (2022).
- [42] I. Mazin (The PRX Editors), Editorial: Altermagnetism—a new punch line of fundamental magnetism, *Phys. Rev. X* **12**, 040002 (2022).
- [43] Z. Feng, X. Zhou, L. Šmejkal, L. Wu, Z. Zhu, H. Guo, R. González-Hernández, X. Wang, H. Yan, P. Qin, *et al.*, An anomalous hall effect in altermagnetic ruthenium dioxide, *Nature Electronics* **5**, 735 (2022).
- [44] I. I. Mazin, Altermagnetism in $mnte$: Origin, predicted manifestations, and routes to detwinning, *Phys. Rev. B* **107**, L100418 (2023).
- [45] P. A. McClarty and J. G. Rau, Landau theory of altermagnetism, *Phys. Rev. Lett.* **132**, 176702 (2024).
- [46] H.-Y. Ma, M. Hu, N. Li, J. Liu, W. Yao, J.-F. Jia, and J. Liu, Multifunctional antiferromagnetic materials with giant piezomagnetism and noncollinear spin current, *Nature communications* **12**, 2846 (2021).
- [47] L. Šmejkal, R. González-Hernández, T. Jungwirth, and J. Sinova, Crystal time-reversal symmetry breaking and spontaneous hall effect in collinear antiferromagnets, *Science advances* **6**,

- eaaz8809 (2020).
- [48] R. González-Hernández, L. Šmejkal, K. Výborný, Y. Yahagi, J. Sinova, T. c. v. Jungwirth, and J. Železný, Efficient electrical spin splitter based on nonrelativistic collinear antiferromagnetism, *Phys. Rev. Lett.* **126**, 127701 (2021).
- [49] H. Bai, L. Han, X. Y. Feng, Y. J. Zhou, R. X. Su, Q. Wang, L. Y. Liao, W. X. Zhu, X. Z. Chen, F. Pan, X. L. Fan, and C. Song, Observation of spin splitting torque in a collinear antiferromagnet RuO_2 , *Phys. Rev. Lett.* **128**, 197202 (2022).
- [50] Y. Fan, Q. Wang, W. Wang, D. Wang, Q. Huang, Z. Wang, X. Han, Y. Chen, L. Bai, S. Yan, *et al.*, Robust magnetic-field-free perpendicular magnetization switching by manipulating spin polarization direction in RuO_2 /[pt/co/pt] heterojunctions, *ACS nano* **18**, 26350 (2024).
- [51] D. B. Litvin and W. Opechowski, Spin groups, *Physica* **76**, 538 (1974).
- [52] D. B. Litvin, Spin point groups, *Acta Crystallographica Section A: Crystal Physics, Diffraction, Theoretical and General Crystallography* **33**, 279 (1977).
- [53] See supplemental material at <http://link.aps.org/supplemental/10.1103/xxx> for computational method, symmetry of transverse electronic conductivity, Brillouin zone and the coordinates of the high symmetry points, isoenergetic surface and comparison of electronic conductivity of RuO_2 with and without SOC, The Supplemental Material also contains Refs. [54-66].
- [54] G. Kresse and D. Joubert, From ultrasoft pseudopotentials to the projector augmented-wave method, *Physical Review B* **59**, 1758 (1999).
- [55] P. E. Blöchl, Projector augmented-wave method, *Physical Review B* **50**, 17953 (1994).
- [56] G. Kresse and J. Furthmüller, Efficient iterative schemes for ab initio total-energy calculations using a plane-wave basis set, *Physical Review B* **54**, 11169 (1996).
- [57] G. Kresse and J. Hafner, Ab initio molecular dynamics for liquid metals, *Physical Review B* **47**, 558 (1993).
- [58] J. P. Perdew, K. Burke, and M. Ernzerhof, Generalized gradient approximation made simple, *Phys. Rev. Lett.* **77**, 3865 (1996).
- [59] G. H. Wannier, The structure of electronic excitation levels in insulating crystals, *Physical Review* **52**, 191 (1937).
- [60] N. Marzari, A. A. Mostofi, J. R. Yates, I. Souza, and D. Vanderbilt, Maximally localized wannier functions: Theory and applications, *Reviews of Modern Physics* **84**, 1419 (2012).
- [61] N. Marzari and D. Vanderbilt, Maximally localized generalized wannier functions for composite energy bands, *Physical Review B* **56**, 12847 (1997).
- [62] A. A. Mostofi, J. R. Yates, Y.-S. Lee, I. Souza, D. Vanderbilt, and N. Marzari, wannier90: A tool for obtaining maximally-localised wannier functions, *Computer Physics Communications* **178**, 685 (2008).

- [63] G. Pizzi, V. Vitale, R. Arita, S. Blügel, F. Freimuth, G. Géranton, M. Gibertini, D. Gresch, C. Johnson, T. Koretsune, J. Ibañez-Azpiroz, H. Lee, J.-M. Lihm, D. Marchand, A. Marrazzo, Y. Mokrousov, J. I. Mustafa, Y. Nohara, Y. Nomura, L. Paulatto, S. Poncé, T. Ponweiser, J. Qiao, F. Thöle, S. S. Tsirkin, M. Wierzbowska, N. Marzari, D. Vanderbilt, I. Souza, A. A. Mostofi, and J. R. Yates, Wannier90 as a community code: new features and applications, *Journal of Physics: Condensed Matter* **32**, 165902 (2020).
- [64] J. M. Ziman, *Principles of the Theory of Solids*, 2nd ed. (Cambridge University Press, 1972).
- [65] G. Grosso and G. P. Parravicini, *Solid state physics* (Academic press, 2013).
- [66] G. Pizzi, D. Volja, B. Kozinsky, M. Fornari, and N. Marzari, Boltzmann: A code for the evaluation of thermoelectric and electronic transport properties with a maximally-localized wannier functions basis, *Computer Physics Communications* **185**, 422 (2014).
- [67] S. Y. Liu, X. L. Lei, and N. J. M. Horing, Vanishing spin-hall current in a diffusive rashba two-dimensional electron system: A quantum boltzmann equation approach, *Phys. Rev. B* **73**, 035323 (2006).
- [68] H. Reichlova, R. Lopes Seeger, R. González-Hernández, I. Kounta, R. Schlitz, D. Kriegner, P. Ritzinger, M. Lammel, M. Leiviskä, A. Birk Hellenes, *et al.*, Observation of a spontaneous anomalous hall response in the mn5si3 d-wave altermagnet candidate, *Nature Communications* **15**, 4961 (2024).
- [69] M. Gottschilch, O. Gourdon, J. Persson, C. de la Cruz, V. Petricek, and T. Brueckel, Study of the antiferromagnetism of mn 5 si 3: an inverse magnetocaloric effect material, *Journal of materials chemistry* **22**, 15275 (2012).
- [70] N. Biniskos, F. Dos Santos, M. dos Santos Dias, S. Raymond, K. Schmalzl, P. Steffens, J. Persson, N. Marzari, S. Blügel, S. Lounis, *et al.*, An overview of the spin dynamics of antiferromagnetic mn5si3, *APL materials* **11** (2023).
- [71] D. Jezierski and W. Grochala, Polymorphism of two-dimensional antiferromagnets, agf₂ and cuf₂, *Phys. Rev. Mater.* **8**, 034407 (2024).
- [72] C. Billy and H. M. Haendler, The crystal structure of copper (ii) fluoride, *Journal of the American Chemical Society* **79**, 1049 (1957).